

Exploring strange nucleon form factors on the lattice

Ronald Babich,¹ Richard C. Brower,^{1,2} Michael A. Clark,³
George T. Fleming,⁴ James C. Osborn,⁵ Claudio Rebbi,^{1,2} and David Schaich²

¹*Center for Computational Science, Boston University,
3 Cummington Street, Boston, MA 02215, USA*

²*Department of Physics, Boston University, 590 Commonwealth Avenue, Boston, MA 02215, USA*

³*Harvard-Smithsonian Center for Astrophysics, 60 Garden Street, Cambridge, MA 02138, USA*

⁴*Department of Physics, Yale University, New Haven, CT 06520, USA*

⁵*Argonne Leadership Computing Facility, 9700 S. Cass Avenue, Argonne, IL 60439, USA*

(Dated: December 2, 2010)

We discuss techniques for evaluating sea quark contributions to hadronic form factors on the lattice and apply these to an exploratory calculation of the strange electromagnetic, axial, and scalar form factors of the nucleon. We employ the Wilson gauge and fermion actions on an anisotropic $24^3 \times 64$ lattice, probing a range of momentum transfer with $Q^2 < 1 \text{ GeV}^2$. The strange electric and magnetic form factors, $G_E^s(Q^2)$ and $G_M^s(Q^2)$, are found to be small and consistent with zero within the statistics of our calculation. The lattice data favor a small negative value for the strange axial form factor $G_A^s(Q^2)$ and exhibit a strong signal for the bare strange scalar matrix element $\langle N | \bar{s}s | N \rangle_0$. We discuss the unique systematic uncertainties affecting the latter quantity relative to the continuum, as well as prospects for improving future determinations with Wilson-like fermions.

PACS numbers: 11.15.Ha 12.38.-t 12.38.Gc 14.20.-c

I. INTRODUCTION

The strange quark is the lightest non-valence quark in the nucleon, and as such provides a unique window into the structure of the proton and neutron. Lattice QCD represents at present the only first-principles predictive method to determine such contributions directly from the underlying theory of the strong interaction. The computational framework for doing this is well established with no fundamental barriers to success. Until recently, however, the calculation of the required quark-line disconnected diagrams was simply too computationally demanding to provide statistically significant results with all uncertainties under control. This is beginning to change. With recent algorithmic advances and continued increases in available computer resources, a new era is dawning where these effects might be determined with precision well beyond both experiment and phenomenological estimates. Here we report on some recent progress toward this goal.

Strange nucleon form factors represent an attractive test case because they have also been the subject of a vigorous experimental program. In particular, a number of collaborations have sought to measure the strange electric and magnetic form factors via parity-violating electron scattering [1, 2], notably SAMPLE, A4, HAPPEX, and G0. Recent combined analyses [3, 4] find values for $G_E^s(Q^2)$ and $G_M^s(Q^2)$ that are small and consistent with zero in the range of momenta so far explored. Also of interest is the strange axial form factor $G_A^s(Q^2)$, to which electron scattering experiments are relatively insensitive. At present, the best constraints come from the two-decades old neutrino scattering data of the E734 experiment at Brookhaven [5]. A recent analysis [6], combining these results with those of HAPPEX and G0, favors a negative value for $G_A^s(Q^2)$ in the range $0.45 < Q^2 < 1.0 \text{ GeV}^2$. These may be compared with the recent MiniBooNE result [7], which is compatible but at the same time consistent with zero.

A special case is presented by the strange axial form factor at zero momentum transfer, $G_A^s(0) = \Delta s$, which may be identified with the strange quark contribution to the spin of the nucleon. This quantity is of particular importance, given the role sea quarks are thought to play in resolving the proton “spin crisis” [8]. In principle, it is accessible in deep inelastic scattering, where it is given by the first moment of the helicity-dependent structure function $\Delta s(x)$. In practice, however, determining the first moment requires an extrapolation of the experimental data to small values of Bjorken x , where uncertainties are less under control. There is some tension between the two most recent analyses from HERMES [9, 10], which rely on different techniques; the former favors a negative value for Δs while the latter finds a result consistent with zero, within somewhat larger uncertainties.

Unlike the strange electromagnetic and axial form factors, the strange scalar form factor $G_S^s(Q^2)$ is not directly accessible to experiment. At zero momentum transfer, this quantity corresponds to the strange scalar matrix element $\langle N | \bar{s}s | N \rangle$. Often considered in relation to the pion-nucleon sigma term [11], it is an important parameter in models of the nucleon. We also note the pivotal role it plays in the interpretation of dark matter experiments. Many models of TeV-scale physics, including the MSSM, yield a dark matter candidate (e.g., neutralino) that scatters from nuclei via Higgs exchange. The Higgs is believed to predominantly couple to strange quarks in the nucleon, since the lighter quarks have proportionally smaller Yukawa couplings while the heavier quarks are too rare to contribute significantly. It follows that the cross section is particularly sensitive to the strange scalar matrix element, which enters through the parameter

$$f_{Ts} = \frac{m_s \langle N | \bar{s}s | N \rangle}{M_N}. \quad (1)$$

As emphasized recently in [12–15], f_{Ts} is poorly known at present and represents the leading theoretical uncertainty in the interpretation of direct detection experiments. A commonly used estimate is that of Nelson and Kaplan [16, 17] (via [14]), who find $f_{Ts} = 0.36(14)$. More recent analyses suggest that the quoted uncertainty may be underestimated [12], and as we discuss further in Section IV A, recent lattice determinations favor a much smaller value. If these results prove to be robust, they would imply that the strange quark is in fact not the dominant contribution, and predicted cross-sections should be substantially smaller as a result [18].

In recent years, there has been a great deal of progress in probing the structure of the nucleon on the lattice [19, 20]. With few exceptions, however, such studies have been restricted to the determination of isovector quantities or otherwise neglect the contribution of “disconnected diagrams,” due to the large cost associated with their evaluation. Nucleon matrix elements involving the strange quark are inherently disconnected, making them an excellent test case for tackling this challenge. Such a matrix element is shown schematically in Figure 1; by “disconnected,” we mean that the diagram includes an insertion on a quark loop that is coupled to the baryon correlator only via the gauge field. This requires the calculation of a trace of the quark propagator over spin, color, and spatial indices. Since an exact calculation would require a number of inversions proportional to the spatial lattice volume, the trace is generally estimated stochastically, which introduces a new source of statistical error whose reduction is discussed in Section II A.

There has been a resurgence of interest lately in computing disconnected form factors on the lattice, building on the pioneering studies of a decade ago [21–29], which were mainly carried out in the quenched approximation. Recent work

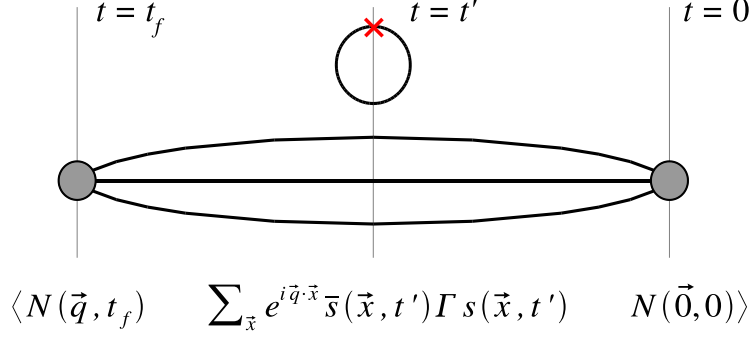


FIG. 1. Schematic representation of a disconnected diagram, giving a strange form factor of the nucleon. Here Γ is the appropriate gamma insertion for the form factor of interest, and N is an interpolating operator for the nucleon.

has included a determination of the nucleon's strange electromagnetic form factors [30], preliminary determinations of Δs [31–35], and several studies of the strange scalar matrix element [31, 33–37]. The latter may also be determined indirectly from the quark mass dependence of the nucleon mass via the Feynman-Hellmann theorem [38–40] or SU(3) chiral perturbation theory [41]. Likewise, a complementary approach for determining the strange electromagnetic form factors relies on combining lattice data for connected form factors with chiral perturbation theory using finite range regularization [42–44]. In this work, we present a direct determination of the strange form factors on relatively large, two-flavor, anisotropic lattices. Some preliminary results were presented in [31, 45].

The paper is organized as follows. In Section II A, we discuss general considerations for computing the disconnected trace and describe the particular approach employed in our calculation. We discuss our approach for extracting form factors from the corresponding matrix elements in Section II B and give further details of the calculation in Section III. In Section IV we present our results for $G_S^s(Q^2)$, $G_A^s(Q^2)$, $G_E^s(Q^2)$, and $G_M^s(Q^2)$. We conclude in Section V with remarks on the steps we are taking to improve future determinations of these quantities.

II. METHOD

A. Evaluating the trace

As discussed in Section I, the evaluation of a disconnected form factor requires the trace of the quark propagator, times some combination of Dirac gamma matrices (Γ) over a time-slice of the lattice. The standard method for estimating such a trace relies on calculating the inverse of the Dirac operator D against an independent set of random vectors $\eta^{(\alpha)}$, $\alpha = 1, \dots, N$ for each spin (i), color (a), and spatial (x) degree of freedom,

$$\text{Tr}(\Gamma D^{-1}) \approx \frac{1}{N} \sum_{\alpha=1}^N \eta^{\dagger(\alpha)} \Gamma D^{-1} \eta^{(\alpha)}, \quad \langle \eta_{i,a,x}^* \eta_{j,b,y} \rangle_{\eta} = \delta_{xy} \delta_{ab} \delta_{ij}. \quad (2)$$

Given a finite ensemble of such noise vectors, this procedure introduces a new source of statistical error, $\pm \sigma / \sqrt{N}$, measured by the variance σ^2 . We note that if we choose an appropriate basis, $\Gamma = (1, \gamma_5, i\gamma_\mu, \gamma_5 \gamma_\mu, i\sigma_{\mu\nu})$, for the Euclidean gamma matrices, γ_5 invariance implies all the traces in Eq. 2 are real. Introducing Gaussian random vectors, the variance for the real part of $O(\eta)$ for large N is

$$\begin{aligned} \sigma^2 &= \frac{1}{4} \left(\langle [O^*(\eta) + O(\eta)]^2 \rangle_{\eta} - \langle O^*(\eta) + O(\eta) \rangle_{\eta}^2 \right) \\ &= \frac{1}{2} \sum_{x,y} \text{tr}[D^{\dagger-1}(x,y) D^{-1}(y,x)] + \frac{1}{2} \sum_{x,y} \text{tr}[\Gamma D^{-1}(x,y) \Gamma D^{-1}(y,x)], \end{aligned} \quad (3)$$

where the operators are $O(\eta) = \eta^{\dagger} \Gamma D^{-1} \eta$ and $\text{tr}[\dots]$ now stands for the trace in spin and color alone. It is also common in practice to introduce “unitary” noise elements in $U(1)$ or Z_2 [46], such that $\eta^* \eta = 1$ which eliminates the diagonal terms corresponding to $x = y$. In either case, the off-diagonal terms for the first term on the right hand side of Eq. 3 fall off exponentially in the space-time separation ($|x - y|$) dictated by the lowest Goldstone pseudoscalar mass in the quark-antiquark channel, giving a divergent variance in the chiral limit. Taking the real part reduced this

divergent term by $1/2$ and substituted more rapidly falling correlators in the second term, except for the pseudoscalar case where $\Gamma = \gamma_5$. In this article we employ two modifications to reduce the variance. Additional methods will be explored in a subsequent publication.

First, we choose a random $SU(3)$ gauge transformation Ω_x as our unitary stochastic vector, with elements drawn from a uniform distribution according to the Haar measure. We also treat the spin contractions exactly, along the lines of the “spin explicit method” described in [47]. As a result, Eq. (2) is replaced by

$$\text{Tr}(\Gamma D^{-1}) \approx \frac{1}{N} \sum_{\alpha=1}^N \text{tr}[\Omega^{\dagger(\alpha)} \Gamma D^{-1} \Omega^{(\alpha)}], \quad \langle \Omega_x^{\dagger ab} \Omega_y^{cd} \rangle_{\Omega} = \delta_{xy} \delta^{ad} \delta^{bc} / 3, \quad (4)$$

and Eq. (3) by

$$\sigma^2 = \frac{1}{2} \sum_{x \neq y} \text{tr}_c \left(\text{tr}_s[D^{\dagger-1}(x, y) \Gamma^{\dagger}] \text{tr}_s[\Gamma D^{-1}(y, x)] \right) + \frac{1}{2} \sum_{x \neq y} \text{tr}_c \left(\text{tr}_s[\Gamma D^{-1}(x, y)] \text{tr}_s[\Gamma D^{-1}(y, x)] \right), \quad (5)$$

where tr_c and tr_s are color and spin traces respectively. Note that all 12 spin/color components in the local term with $x = y$ are removed from the variance. In addition, the explicit spin sum results in separating the $SU(3)$ gauge trace from the Dirac (spin) trace for each propagator. The variance depends on the individual gamma structure and as a result in general falls off faster for large $|x - y|$ than the lowest Goldstone mode. To determine the specific quark/anti-quark channel that contributes, one must perform a Fierz transformation on each term to put the gamma matrices in the conventional position for a meson two-point function. There will be only one linear combination affected by the Goldstone mode. The other 15 combinations are determined by massive meson channels even in the chiral limit. We leave a more detailed analysis to a future publication dealing with the light quark sector where this becomes a more critical issue.

Second, we introduce *dilution* to reduce the variance, by dividing the stochastic source into subsets and estimating the trace on each subset separately [48, 49]. As a simple illustration consider even/odd dilution, which involves two subsets,

$$\text{Tr}(\Gamma D^{-1}) \approx \frac{1}{N} \sum_{\alpha=1}^N \eta_e^{(\alpha)\dagger} \Gamma D^{-1} \eta_e^{(\alpha)} + \frac{1}{N} \sum_{\alpha=1}^N \eta_o^{(\alpha)\dagger} \Gamma D^{-1} \eta_o^{(\alpha)}, \quad (6)$$

where $\eta_e^{(\alpha)}$ and $\eta_o^{(\alpha)}$ are non-zero only on the even and odd sites, respectively, and $\eta_e^{(\alpha)} + \eta_o^{(\alpha)} = \eta^{(\alpha)}$ gives the original noise vector. This may be generalized to a more aggressive dilution pattern where a larger number of diluted sources is used, each more sparse. The lighter the quark mass the more aggressively one should use dilution. We combine such a scheme with $SU(3)$ unitary noise and an exact treatment of the spin sum. Note that had we instead used dilution over the color index, the resulting variance would no longer be gauge invariant.

A full calculation involves two sources of statistical error: the usual gauge noise and the error in the trace. In this investigation for the strange quark, we largely eliminate the latter error by calculating a “nearly exact” trace on each of four time-slices with very aggressive dilution. This is accomplished by employing a large number of sources (864×12 for color/spin on a $24^3 \times 64$ lattice) where each source is nonzero on only 16 sites on each of the four time-slices. The sites are chosen such that the smallest spatial separation between them is $6\sqrt{3}a_s$. With this aggressive dilution pattern, we find that it is sufficient to use a single $SU(3)$ source per subset, provided automatically by the random gauge noise in stochastically independent configurations of our ensemble. Any residual contamination, which we observe to be small, is gauge-variant and averages to zero. We note that apart from our use of dilution, this approach corresponds to the “wall source without gauge fixing” method employed in some of the earliest investigations of disconnected form factors [21, 22].

B. Lattice correlation functions

In Minkowski space, the familiar Dirac and Pauli form factors of the nucleon, $F_1(Q^2)$ and $F_2(Q^2)$, are implicitly defined by

$$\langle N(p') | J_{\mu} | N(p) \rangle = \bar{u}(p') \left[\gamma_{\mu} F_1(Q^2) + \frac{i \sigma_{\mu\nu} q^{\nu}}{2m} F_2(Q^2) \right] u(p). \quad (7)$$

Here $|N(p)\rangle$ is a nucleon state with momentum p , $u(p)$ is a nucleon spinor, and we define $Q^2 = -q^2$, where $q = p' - p$ is the 4-momentum transfer. It is often convenient to consider instead the Sachs electric and magnetic form factors,

given by

$$G_E(Q^2) = F_1(Q^2) - \frac{Q^2}{4M^2} F_2(Q^2) \quad (8)$$

and

$$G_M(Q^2) = F_1(Q^2) + F_2(Q^2), \quad (9)$$

respectively. The contribution of an individual quark flavor (e.g., the strange quark) is defined by replacing the full electromagnetic current that appears in Eq. (7),

$$J_\mu = \frac{2}{3} \bar{u} \gamma_\mu u - \frac{1}{3} \bar{d} \gamma_\mu d - \frac{1}{3} \bar{s} \gamma_\mu s + \dots, \quad (10)$$

by $J_\mu^s = \bar{s} \gamma_\mu s$. The corresponding Sachs electric and magnetic form factors are denoted by $G_E^s(Q^2)$ and $G_M^s(Q^2)$, respectively.

Similarly, the strange quark contribution to the axial form factor of the nucleon, $G_A^s(Q^2)$, is implicitly given by

$$\langle N(p') | \bar{s} \gamma_\mu \gamma_5 s | N(p) \rangle = \bar{u}(p') \left[\gamma_\mu \gamma_5 G_A^s(Q^2) + \frac{q_\mu}{2m} \gamma_5 G_P^s(Q^2) \right] u(p). \quad (11)$$

In this equation $G_P^s(Q^2)$ denotes the strange quark contribution to the induced pseudoscalar form factor of the nucleon, which we will not consider further here. Finally, we note that the strange scalar form factor is trivially given by $G_S^s(Q^2) = \langle N(p') | \bar{s} s | N(p) \rangle$. Our main focus will be on the special case of $Q^2 = 0$, with the matrix element denoted simply by $\langle N | \bar{s} s | N \rangle$.

Our task is to extract these four quantities from appropriately defined Euclidean correlation functions on the lattice. We begin by defining the usual two-point function for the nucleon, with momentum \vec{q} ,

$$G^{(2)}(t, t_0; \vec{q}) = (1 + \gamma_4)^{\alpha\beta} \sum_{\vec{x}} e^{i\vec{q} \cdot \vec{x}} \langle N^\beta(\vec{x}, t) \bar{N}^\alpha(\vec{0}, t_0) \rangle. \quad (12)$$

Here $N^\alpha = \epsilon_{abc} (u_a^T C \gamma_5 d_b) u_c^\alpha$ is the standard interpolating operator for the proton, with smeared quark fields, and $(1 + \gamma_4)$ projects out the positive-parity state. In everything that follows, we always double our statistics by making use of the invariance of the action under time reversal. More concretely, in this case we combine the “forward-propagating” correlator $G^{(2)}(t, t_0; \vec{q})$ with the backward-propagating $G_-^{(2)}(t_0, t; \vec{q})$, where the “−” subscript indicates that $(1 + \gamma_4)$ in Eq. (12) has been replaced by $(1 - \gamma_4)$.

Next, we define various three-point functions $G_X^{(3)}(t, t', t_0; \vec{q})$, where $X = S, A, E, M$ correspond to the disconnected scalar, axial, electric, and magnetic form factors, respectively. These are given by

$$G_S^{(3)}(t, t', t_0; \vec{q}) = (1 + \gamma_4)^{\alpha\beta} \sum_{\vec{x}, \vec{x}'} e^{i\vec{q} \cdot \vec{x}'} \langle N^\beta(\vec{x}, t) [\bar{\psi} \psi(\vec{x}', t') - \langle \bar{\psi} \psi(\vec{x}', t') \rangle] \bar{N}^\alpha(\vec{0}, t_0) \rangle \quad (13)$$

for the scalar,

$$G_A^{(3)}(t, t', t_0; \vec{q}) = \frac{1}{3} \sum_{i=1}^3 \sum_{\vec{x}, \vec{x}'} e^{i\vec{q} \cdot \vec{x}'} [-i(1 + \gamma_4) \gamma_i \gamma_5]^{\alpha\beta} \langle N^\beta(\vec{x}, t) [A_i(\vec{x}', t') - \langle A_i(\vec{x}', t') \rangle] \bar{N}^\alpha(\vec{0}, t_0) \rangle \quad (14)$$

for the axial,

$$G_E^{(3)}(t, t', t_0; \vec{q}) = (1 + \gamma_4)^{\alpha\beta} \sum_{\vec{x}, \vec{x}'} e^{i\vec{q} \cdot \vec{x}'} \langle N^\beta(\vec{x}, t) [V_4(\vec{x}', t') - \langle V_4(\vec{x}', t') \rangle] \bar{N}^\alpha(\vec{0}, t_0) \rangle \quad (15)$$

for the electric, and

$$G_M^{(3)}(t, t', t_0; \vec{q}) = \frac{1}{2n_q} \sum_{\substack{i,j,k \\ q_j \neq 0}} \epsilon_{ijk} \frac{1}{q_j} \sum_{\vec{x}, \vec{x}'} e^{i\vec{q} \cdot \vec{x}'} [-i(1 + \gamma_4) \gamma_i \gamma_5]^{\alpha\beta} \langle N^\beta(\vec{x}, t) [V_k(\vec{x}', t') - \langle V_k(\vec{x}', t') \rangle] \bar{N}^\alpha(\vec{0}, t_0) \rangle \quad (16)$$

for the magnetic. Here V_μ and A_μ denote the vector and axial currents, and n_q in Eq. (16) simply counts the number of nonzero components of \vec{q} . For V_μ , we utilize the conserved current for the Wilson action, given by

$$V_\mu(x + a_\mu \hat{\mu}/2) = \frac{1}{2} [\bar{\psi}(x + a_\mu \hat{\mu})(\gamma_\mu + 1) U_\mu^\dagger(x) \psi(x) + \bar{\psi}(x)(\gamma_\mu - 1) U_\mu(x) \psi(x + a_\mu \hat{\mu})] . \quad (17)$$

The lattice spacing carries a label μ because we will consider anisotropic lattices for which the temporal lattice spacing, $a_4 \equiv a_t$, differs from the spatial lattice spacing, $a_1 = a_2 = a_3 \equiv a_s$. For convenience, we define $V_\mu(x)$ on a given site of the lattice by averaging those terms involving the adjacent forward and backward links, $V_\mu(x) \equiv [V_\mu(x + a_\mu \hat{\mu}/2) + V_\mu(x - a_\mu \hat{\mu}/2)]/2$; since the spatial index determines the phase in the Fourier transform, this corresponds to an $\mathcal{O}(a^2 q^2)$ redefinition of the three-point function. For the axial form factor, we will present results computed both from the analogous point-split current,

$$A_\mu^{(\text{p.s.})}(x + a_\mu \hat{\mu}/2) = \frac{i}{2} [\bar{\psi}(x + a_\mu \hat{\mu}) \gamma_\mu \gamma_5 U_\mu^\dagger(x) \psi(x) + \bar{\psi}(x) \gamma_\mu \gamma_5 U_\mu(x) \psi(x + a_\mu \hat{\mu})], \quad (18)$$

and the standard local current, $A_\mu^{(\text{local})}(x) = i\bar{\psi}(x) \gamma_\mu \gamma_5 \psi(x)$.

Note that in Eq. (13)-(16) we always employ the vacuum-subtracted value of the current, $[J(\vec{x}, t) - \langle J(\vec{x}, t) \rangle]$, even though this is only strictly necessary when J is the scalar density, since the expectation value of the others vanish. Given finite statistics, however, and an inexact estimate of the trace, it is possible that using the vacuum-subtracted value gives reduced statistical errors. Empirically, we find that for the strange axial form factor at $Q^2 = 0$, the two approaches give indistinguishable results. At larger momenta, however, uncertainties for the vacuum-subtracted quantities are noticeably smaller.

To interpret our results, we require an understanding of the correlation functions given in Eqs. (13)-(16) in terms of the lowest one or two states that dominate at large times. This is accomplished by performing a spectral decomposition in the transfer matrix formalism, and for the nucleon two-point function given in Eq. (12), we find

$$G^{(2)}(t, t_0; \vec{q}) = \sum_n 2 \left(1 + \frac{m_n}{E_n} \right) Z_n^2(\vec{q}) e^{-E_n(t-t_0)}. \quad (19)$$

Here $Z_n(\vec{p})$ is defined by $\langle n, \vec{p}, s | \bar{N}^\alpha(\vec{0}) | 0 \rangle = Z_n(\vec{p}) \bar{u}_s^\alpha(\vec{p})$, where $\bar{N}^\alpha(\vec{x})$ is a creation operator for the nucleon, $|n, \vec{p}, s\rangle$ is its n th eigenstate (with momentum \vec{p} and polarization s), and we have adopted a relativistic normalization convention for the states: $\langle n', \vec{p}', s' | n, \vec{p}, s \rangle = 2E_n(\vec{p}) L^3 \delta_{s,s'} \delta_{\vec{p},\vec{p}}^{(3)}$. The momentum dependence in $Z_n(\vec{p})$ arises because we will generally consider extended, rather than point-like, operators. We take $n = 1$ to label the ground-state proton, and for later convenience we collect together the coefficients,

$$c_n(\vec{q}) = 2 \left(1 + \frac{m_n}{E_n} \right) Z_n^2(\vec{q}), \quad (20)$$

yielding

$$G^{(2)}(t, t_0; \vec{q}) = \sum_n c_n(\vec{q}) e^{-E_n(t-t_0)}. \quad (21)$$

Similarly, for a generic three-point function involving a current $J_X(\vec{x}, t)$,

$$G_X^{(3)}(t, t', t_0; \vec{q}) = \Gamma_X^{\alpha\beta} \sum_{\vec{x}, \vec{x}'} e^{i\vec{q} \cdot \vec{x}'} \langle N^\beta(\vec{x}, t) J_X(\vec{x}', t') \bar{N}^\alpha(\vec{0}, t_0) \rangle, \quad (22)$$

we find

$$G_X^{(3)}(t, t', t_0; \vec{q}) = \sum_{m,n} j_{nm}(\vec{q}) e^{-m_n(t-t')} e^{-E_m(\vec{q})(t'-t_0)}, \quad (23)$$

where the coefficients j_{nm} may generally be expressed in terms of suitable form factors, depending on the current J_X and the combination of gamma matrices Γ_X . The correlation functions in Eq. (13)-(16) have been constructed such that in each case, the ground-state coefficient j_{11} may be simply expressed in terms of a single form factor. In particular, for $X = S, A, E$, we have

$$j_{11}(\vec{q}) = 2 \left(1 + \frac{m_1}{E_1(\vec{q})} \right) Z_1(\vec{0}) Z_1(\vec{q}) G_X^s(Q^2), \quad (24)$$

where $G_X^s(Q^2)$ is the corresponding strange form factor of the nucleon. For the magnetic case, the appropriate expression is

$$j_{11}(\vec{q}) = \frac{2}{E_1(\vec{q})} Z_1(\vec{0}) Z_1(\vec{q}) G_M^s(Q^2). \quad (25)$$

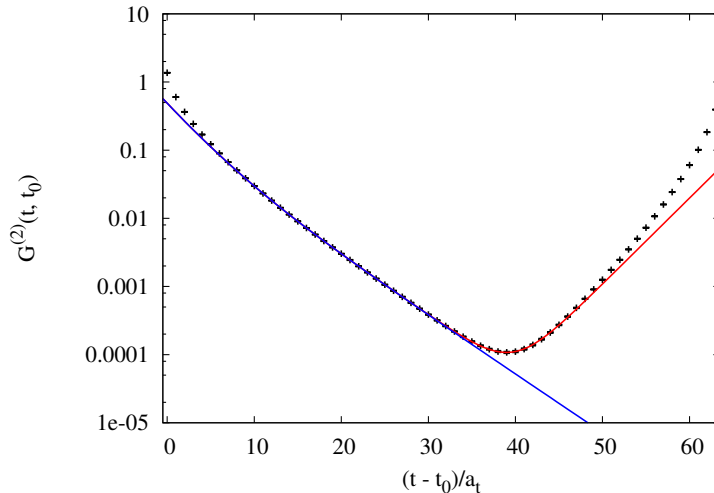


FIG. 2. Fit of the nucleon correlation function for $Q^2 = 0$ to a form that includes two forward-propagating states and one backward-propagating state (upper curve, red) and the same form with the coefficient of the backward-propagating set to zero but the other fit parameters held fixed (lower curve, blue).

III. DETAILS OF THE CALCULATION

We work on a $24^3 \times 64$ anisotropic lattice, utilizing an ensemble of 863 gauge field configurations provided by the Hadron Spectrum Collaboration [50]. These were generated with two degenerate flavors in the sea. Our gauge and fermion actions are those defined in Appendix A, with coupling $\beta = 6/g^2 = 5.5$ and bare anisotropy $\xi_0 = 2.38$. In [50], it was found that this value of ξ_0 together with $\nu = 1$ gives renormalized gauge and fermion anisotropies that are consistent with $\xi = 3$.

The spatial lattice spacing was determined from the Sommer scale [51] with the parameter $r_0 = 0.462(11)(4)$ fm, taken from [52, 53], yielding $a_s = 0.108(7)$ fm $= 3a_t$. For the light quarks, the mass parameter m_l^0 that appears in the action is $m_l^0 = -0.4125$. The corresponding pion mass is $M_\pi = 416(36)$ MeV [50].

Given the anisotropy, our lattice has a relatively short extent in time, which has influenced our choice of method. It has been conventional in lattice studies to extract the form factors by considering various ratios of the three- and two-point functions defined above. For example, at zero momentum transfer, one finds

$$R_X(t, t', t_0; Q^2 = 0) \equiv \frac{G_X^{(3)}(t, t', t_0; \vec{0})}{G^{(2)}(t, t_0; \vec{0})} \rightarrow G_X^s(Q^2 = 0), \quad (26)$$

for large time separations. Instead, we have chosen to fit the three-point function that appears in the numerator of this ratio directly. The reasons are two-fold. First, this allows us to avoid contamination from backward-propagating states, which are problematic due to the short temporal extent of our lattice. At the same time, it allows us to explicitly take into account the contribution of (forward-propagating) excited states.

To see why the direct approach avoids the problem of finite-time contamination, note that this contamination chiefly affects the nucleon correlator $G^{(2)}(t, t_0; \vec{0})$ that appears in the denominator of Eq. (26), since it involves propagation for a time $(t - t_0)$. As $(t - t_0)$ exceeds $L_t/2$, the correlator becomes progressively more contaminated by the negative-parity partner of the nucleon propagating backward through the lattice. In Figure 2, we show a plot of the nucleon correlator, together with a fit to a functional form that includes two forward-going states and one backward-going state. The lower curve shows the effect of dropping the term that corresponds to the latter; we use this for normalizing some of our results at zero momentum transfer when we plot them below.

As a result of the contamination in the denominator, the ratio R_X begins to decrease precipitously at large times. It is important to note that although $G_X^{(3)}(t, t', t_0; \vec{q})$ in the numerator also involves a nucleon propagating for time $(t - t_0)$, the contamination there is a concern only insofar as it increases the statistical error by washing out the correlation we are attempting to measure. It remains unbiased since the current is inserted at t' , while the negative-parity partner propagates across the opposite side of the lattice, from t to t_0 , and can be expected to correlate little with the disconnected insertion.

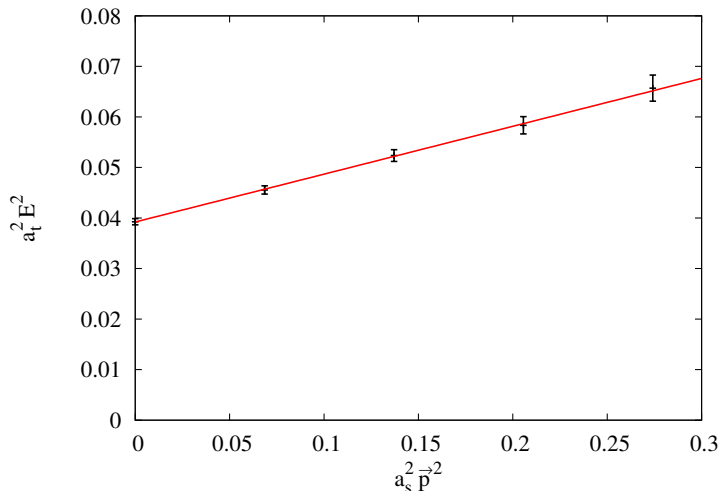


FIG. 3. Nucleon energy-squared (in lattice units) as a function of momentum, together with a fit to the continuum dispersion relation.

As described in the previous section, the correlation functions given in Eqs. (13)-(15) have been defined such that a single form factor enters the coefficient j_{11} for each case, according to Eq. (24). In terms of the coefficients c_n extracted from the two-point function $G^{(2)}(t, t_0; \vec{q})$, this becomes

$$j_{11}(\vec{q}) = G_X^s(Q^2) \sqrt{\frac{1}{2} \left(1 + \frac{m_1}{E_1(\vec{q})} \right)} c_1(\vec{0}) c_1(\vec{q}) \quad (27)$$

for $X = S, E, A$, where $G_X^s(Q^2)$ is the corresponding strange form factor of the nucleon. The corresponding expression for $G_M^{(3)}(t, t', t_0; \vec{q})$ is

$$j_{11}(\vec{q}) = \frac{G_M^s(Q^2)}{E_1(\vec{q}) + m_1} \sqrt{\frac{1}{2} \left(1 + \frac{m_1}{E_1(\vec{q})} \right)} c_1(\vec{0}) c_1(\vec{q}). \quad (28)$$

Our general strategy will be to fit the correlation functions $G_X^{(3)}(t, t', t_0; \vec{q})$ to Eq. (23), taking into account both the ground state nucleon and a single excited state. We may then extract the nucleon form factors from j_{11} with input from the two-point function. In principle, one could also obtain form factors of the first excited state from j_{22} , as well as transition form factors from j_{12} and j_{21} . In practice, however, we expect these to absorb the contributions of still higher states and trust only the ground state form factors to be reliable.

IV. RESULTS AND DISCUSSION

A. Strange scalar form factor and f_{Ts}

For all of the results presented in this section, the nucleon two-point function was fit in the range $10 \leq t/a_t \leq 45$, yielding $a_t M_N = 0.198(2)$ for the ground-state nucleon mass. In Figure 3, we plot the nucleon energy (squared) as a function of momentum for the five smallest values of $|\vec{p}|^2$ available on our lattice, along with a fit to the continuum dispersion relation $(a_t E)^2 = (a_s |\vec{p}|)^2 / \xi^2 + (a_t m)^2$. The parameter ξ , given by the inverse square root of the slope, provides a measure of the effective fermion anisotropy a_s/a_t . We find $\xi = 3.25(11)$ from the fit, which may be compared to the values 2.979(28) and 3.045(35) obtained from the pion and rho dispersion relations, respectively, in [50]. The intercept $(a_t m)^2$ in Figure 3 is largely constrained by the point at $|\vec{p}|^2 = 0$ and thus yields an identical value (and error) for the nucleon mass.

In order to extract the form factors, the various three-point functions were fit to Eq. (23), taking into account the two lowest-lying states, with the separations $(t - t')/a_t$ and $(t' - t_0)/a_t$ varying independently in the range [10, 18]. It

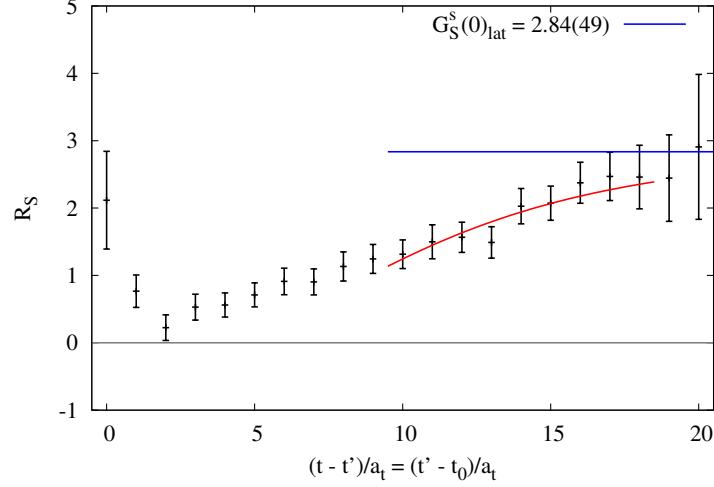


FIG. 4. Subset of results for the scalar form factor at $Q^2 = 0$, where the current insertion is placed symmetrically between source and sink. The lower curve (red) shows a corresponding cross-section of the fit. The horizontal line (blue) indicates the resulting value of $G_S^s(Q^2 = 0)_{\text{lat}} = \langle N | \bar{s}s | N \rangle_0$ for the ground-state nucleon.

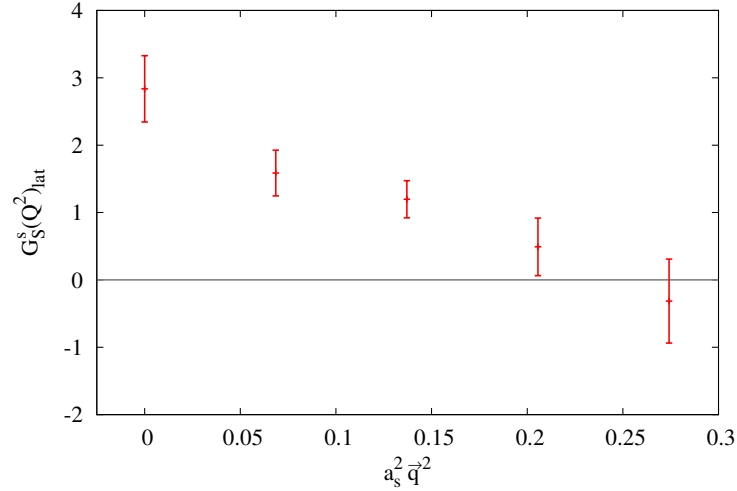


FIG. 5. Strange scalar form factor as a function of momentum.

follows that a total of 81 data points are included in the fit. A one-dimensional subset of these points for the scalar form factor at $Q^2 = 0$ is shown in Figure 4. For the purpose of plotting, we have normalized our results by a fit to the two-point function. With this normalization, dominance of the ground state should manifest as a plateau at large times. We find $G_S^s(0)_{\text{lat}} = 2.84(49)$ for the form factor at zero momentum transfer, where the statistical error has been determined via a single-elimination jackknife applied to the full fitting procedure. In Figure 5, we show the momentum dependence of the strange scalar form factor.

We discuss the systematic uncertainties affecting these results below, including the delicate problem of relating the bare matrix element to the continuum. One practical consideration is the choice of fitting windows used in the fits of the two- and three-point functions. In order to extract the form factors from $G_X^{(3)}(t, t', t_0; \vec{q})$, we must first determine the coefficients $c_n(\vec{q})$ and masses/energies $E_n(\vec{q})$ from a fit to $G^{(2)}(t, t_0; \vec{q})$. Since we have access to a total of $863 \times 64 = 55,232$ nucleon correlators, these tend to be very well-determined, as illustrated by Figure 2. The coefficients c_n are somewhat sensitive to the choice of fitting window, however, and since they multiply the form factor in Eq. (27), this translates into a direct systematic error on the form factor, estimated to be about ten percent.

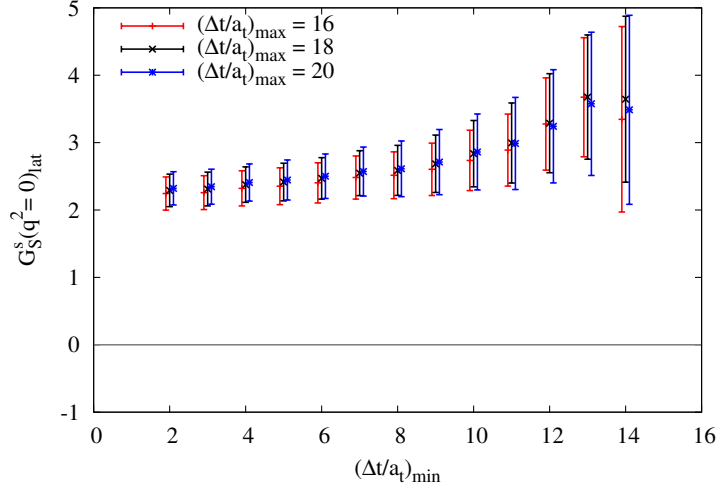


FIG. 6. Dependence of the extracted value of $G_S^s(Q^2 = 0)_{\text{lat}} = \langle N | \bar{s}s | N \rangle_0$ on the range of time separations included in the fit.

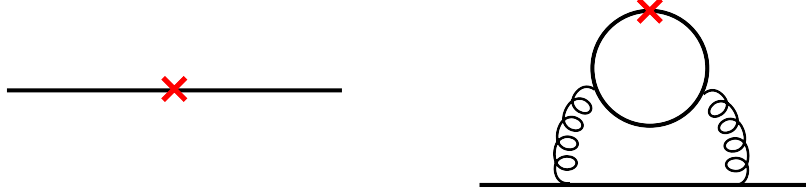


FIG. 7. The left diagram contributes to the renormalization of both the flavor singlet and flavor non-singlet mass operator, while the right appears only for the flavor singlet case.

In contrast, we find that our results are relatively insensitive to the choice of window used in the fit of the three-point function. This is illustrated in Figure 6, where we plot the extracted value of $G_S^s(Q^2 = 0)_{\text{lat}} = \langle N | \bar{s}s | N \rangle_0$ as a function of the smallest time separation included in the fit, for three different values of the maximum time separation. (See also the analogous plot for $G_A^s(Q^2 = 0)$, Figure 12 below.) We observe a stable plateau that extends to very early time separations but have nevertheless chosen a conservative lower bound, $(t - t') \geq 10a_t$ and $(t' - t_0) \geq 10a_t$, effectively eliminating systematics due to excited-state contamination of the three-point function, at the expense of increased statistical errors.

Thus far, we have computed only the unrenormalized matrix element $\langle N | \bar{s}s | N \rangle_0$ on the lattice. Naively we can multiply by the subtracted bare strange quark mass $\tilde{m}_s^0 = m_s^0 - m_{\text{crit}}$ (determined in Appendix B), to find $(\sigma_s)_{\text{lat}} = 504(91)(30)$ MeV, which in the continuum corresponds to the renormalization group invariant quantity $\sigma_s = m_s \langle N | \bar{s}s | N \rangle$. Here the second error reflects the uncertainty in the lattice scale, the first is statistical, and no other systematics have been taken into account. If we then divide by our measured value of the nucleon mass, $a_t M_N = 0.198(2)$, the lattice spacing dependence drops out, yielding $(f_{T_s})_{\text{lat}} = \tilde{m}_s^0 \langle N | \bar{s}s | N \rangle_0 / M_N = 0.46(9)$. This large value is in apparent disagreement with recent lattice determinations using staggered and chiral fermions [36, 37, 39, 40]. The source of this discrepancy, as first pointed out in [38], is the explicit breaking of chiral symmetry in the Wilson action, which allows for mixing between singlet and non-singlet matrix elements even after tuning the quark masses $\tilde{m}_i^0 = m_i^0 - m_{\text{crit}}$ to zero. As a consequence, at finite lattice spacing the strange scalar matrix element receives contributions from both connected and disconnected diagrams involving the *light* quarks, such as those illustrated in Figure 7.

As described in [54, 55] in the context of quark mass renormalization, a natural approach for treating this problem is to separately consider the renormalization of flavor singlet and non-singlet contributions. In Appendix C, we employ this approach with the aid of the lattice Feynman-Hellmann theorem to rederive a result recently quoted in [37] for

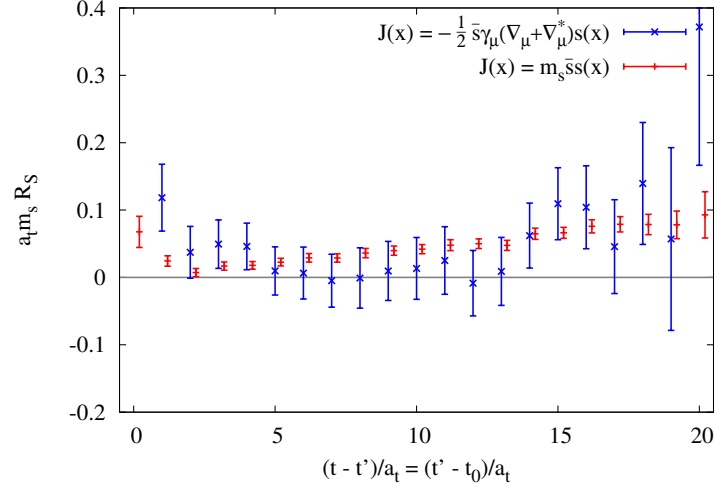


FIG. 8. Determination of $\sigma_s = m_s \langle N | \bar{s}s | N \rangle$ (in lattice units) from the discretized “kinetic term,” as compared to same quantity evaluated by direct insertion of the scalar density multiplied by the subtracted bare quark mass.

the renormalized matrix element,

$$\langle N | \bar{s}s | N \rangle = \frac{1}{3} [(Z_0 + 2Z_8) \langle N | \bar{s}s | N \rangle_0 + (Z_0 - Z_8) \langle N | \bar{u}u + \bar{d}d | N \rangle_0] + c \langle N | \text{Tr}[F^2] | N \rangle_0. \quad (29)$$

Here Z_0 and Z_8 are the flavor singlet and non-singlet renormalization constants for the scalar density, $\text{Tr}[F^2]$ is the gauge kinetic term, and c is a constant. The discussion in Appendix C closely parallels the analysis of Bhattacharya, Gupta, Lee, Sharpe, and Wu [56], who consider in detail operator mixing for $N_f = 2 + 1$ clover-improved Wilson fermions with $m_d = m_u < m_s$, including all terms to $O(a)$ and $O(am_q)$. This is a generalization of the classic on-shell $O(a)$ improvement scheme of the ALPHA collaboration [57, 58].

A self-consistent application of this approach demands an $O(a)$ -improved action with $2 + 1$ dynamical flavors in the sea; such a calculation is under way (see conclusion) but beyond the scope of this paper. Nonetheless the discussion in Appendix C is intended to clarify the source of the mixing problem. In accordance with [54–56], it demonstrates that the singlet (Z_0^m) and non-singlet (Z_8^m) mass renormalization constants separately obey the reciprocal relations $Z_0^m = 1/Z_0$ and $Z_8^m = 1/Z_8$ at zero quark mass and indicates why one expects the gluonic mixing (parameterized by c) to be small. In the approximation where the gluonic mixing is neglected ($c = 0$), correcting the dimensionless ratio $f_{T_s} = m_s \langle N | \bar{s}s | N \rangle / M_N$ only requires computation of the ratio Z_8/Z_0 . Consequently, we believe the value for the renormalization of the condensates can in principle be estimated following the prescription outlined in [54, 55]; by varying the valence and sea quark mass separately one can separate out the singlet and non-singlet contributions. Alternatively, one could determine this ratio by evaluating singlet and non-singlet matrix elements directly. Details of how best to compute the corrections are left for a future work. Suffice it to say that since the corrections due to mixing are large and negative (i.e., $Z_8/Z_0 > 1$), we cannot rule out the possibility that the renormalized quantity $\langle N | \bar{s}s | N \rangle$ is consistent with zero within errors for the present calculation.

We now consider an alternative method for determining $\sigma_s = m_s \langle N | \bar{s}s | N \rangle$ by invoking the continuum equations of motion to replace $m_s \bar{s}s$ by the quark “kinetic term,” $\bar{s} \gamma_\mu D_\mu s$. On the lattice, the covariant derivative goes over to $D_\mu = (\nabla_\mu + \nabla_\mu^*)/2$, defined in terms of the covariant finite difference operators ∇_μ and ∇_μ^* given in Appendix A. Evaluating the matrix element of this operator gives us an alternative determination of σ_s , with lattice artifacts that are at least different and potentially less severe than those affecting the direct approach. In particular, this alternative obviates the need to separately consider quark mass and operator subtractions. Before turning to our results, we note that by splitting the lattice Wilson Dirac operator into three pieces,

$$D = \gamma_\mu D_\mu[U] + m_0^i + W[U] \quad (30)$$

corresponding to the kinetic term, the bare mass term, and the Wilson term, respectively, and by invoking the exact lattice equation of motion, we may write this matrix element in two equivalent ways:

$$-\langle N | \bar{s} \gamma_\mu D_\mu s | N \rangle = \langle N | (m_s^0 \bar{s}s + \bar{s} W s) | N \rangle. \quad (31)$$

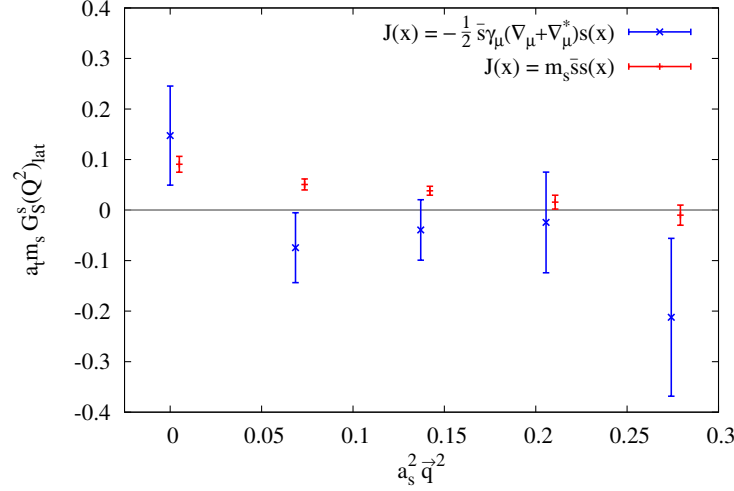


FIG. 9. Momentum dependence of $a_t m_s G_S^s(Q^2)$, as determined directly and from the kinetic term.

From the expression on the right, we see that we have in effect subtracted the major shift due to m_{crit} . Indeed an alternative definition of the critical mass follows from imposing the condition,

$$\langle N | (m_s^0 \bar{s}s + \bar{s}W s) | N \rangle = (m_s^0 - \hat{m}_{\text{crit}}) \langle N | \bar{s}s | N \rangle \quad (32)$$

where $\hat{m}_{\text{crit}} \equiv -\langle N | \bar{s}W s | N \rangle / \langle N | \bar{s}s | N \rangle$. With this definition, at $m_s^0 = \hat{m}_{\text{crit}}$ the flavor singlet term in Figure 7 is set to zero, suggesting that this scheme may suffer from smaller operator mixing than the direct approach.

A practical question is how the statistical uncertainties in the two approaches compare. In Figure 8, we show our results for σ_s determined from the matrix element of the kinetic term. For comparison, we also include the data for $\langle N | \bar{s}s | N \rangle_0$ shown previously in Figure 4, but now rescaled by the bare subtracted quark mass (using the standard definition computed in Appendix B). If not for lattice artifacts, these two sets of results would correspond to the same continuum quantity. We find that the determination from the kinetic term does in fact suffer from much larger statistical errors, perhaps limiting the usefulness of the approach. A final judgement should await comparison of properly subtracted and renormalized results; such an investigation is underway. For completeness, Figure 9 shows results for the scalar form factor as a function of momentum using the two approaches. The points with smaller error bars correspond to the data of Figure 5, rescaled by the bare subtracted quark mass.

B. Strange axial form factor and Δs

Results for the strange axial form factor are shown in Figure 10, here computed using the point-split current of Eq. (18). As was the case for $G_S^s(Q^2)$, we note that our result $(\Delta s)_{\text{lat}} = G_A^s(0)_{\text{lat}} = -0.019(11)$ has not been renormalized and so may not be compared directly to experimental results.¹ Despite the large errors, the data in Figure 10 seem to strongly favor a negative value for Δs , an observation that is in itself of phenomenological interest, given the present uncertainties in experimental determinations and the continued disagreement among some model calculations over the sign. In Figure 11, we show the momentum dependence of $G_A^s(Q^2)$. Because the determination of renormalization constants for our anisotropic lattice action is still pending, we present results for both the point-split and local axial currents.

Finally, Figure 12 shows how the extracted value of $G_A^s(Q^2 = 0)$ would vary as a function of the range of time separations included in the fit. As described earlier, in computing all our results we have chosen a conservative range with the time separations $(t - t')/a_t$ and $(t' - t_0)/a_t$ varying independently in the interval $[10, 18]$. The corresponding point in the figure is labeled by $(\Delta t/a_t)_{\text{min}} = 10$ and $(\Delta t/a_t)_{\text{max}} = 18$.

¹ We also note that the preliminary results for the bare quantity $G_A^s(0)_{\text{lat}}$ reported in [31] were computed using a point-split current involving gauge links rescaled by the bare anisotropy, $\xi_0 = 2.38$. Here we adopt a more conventional normalization for the current, for which $Z_A \sim 1$.

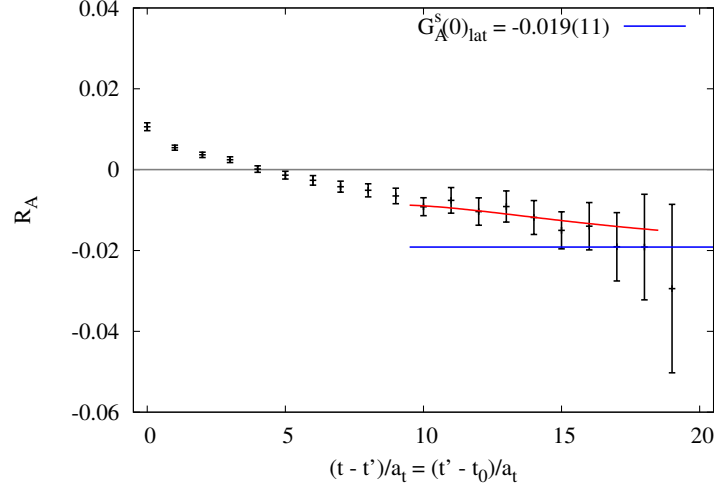


FIG. 10. Subset of results for the axial form factor at $Q^2 = 0$, where the current insertion is placed symmetrically between source and sink. The lower curve (red) shows a corresponding cross-section of the fit. The horizontal line (blue) indicates the resulting value of $G_A^s(Q^2 = 0)_{\text{lat}} = (\Delta s)_{\text{lat}}$ for the ground-state nucleon.

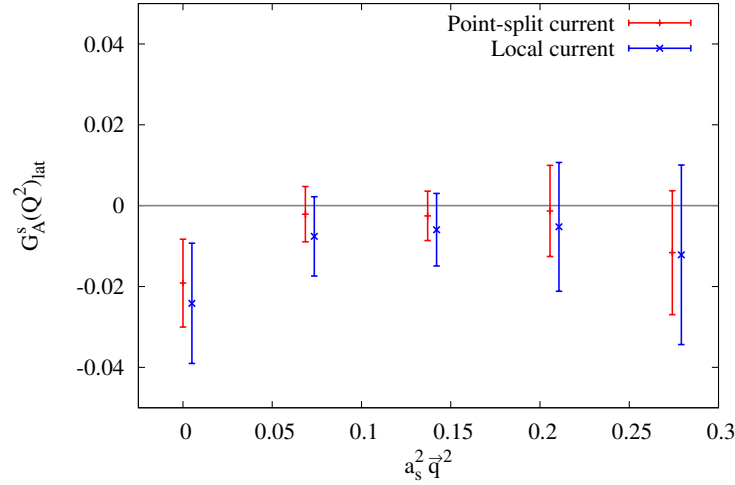


FIG. 11. Strange axial form factor as a function of momentum.

C. Strange electric and magnetic form factors

In Figure 13, we present our results for the strange quark contribution to the nucleon's electric and magnetic form factors, as a function of momentum. We have used the vector current defined in Eq. 17, which is conserved for the Wilson action and therefore does not get renormalized. Note that since the strange quark does not contribute to the electric charge of the nucleon, $G_E^s(Q^2 = 0)$ must vanish. This provides an additional check of our method, and we find $G_E^s(Q^2 = 0) = -0.0016(20)$, consistent with zero as expected. More generally, all of our results for $G_E^s(Q^2)$ and $G_M^s(Q^2)$ appear to be roughly consistent with zero, implying that these quantities are rather small for $Q^2 > 0.1 \text{ GeV}^2$. Strictly speaking, we cannot set proper limits without extrapolating our results to the continuum and to the physical value of the light quark mass, but it is notable that the statistical errors are as much as an order of magnitude smaller than the corresponding experimental uncertainties (cf. [6, 59]). This suggests that measuring a nonzero value for $G_{E,M}^s(Q^2)$ in electron scattering experiments may be a challenging task indeed.

In Table I, we summarize our results for the strange form factors of the nucleon, with the momentum transfer Q^2

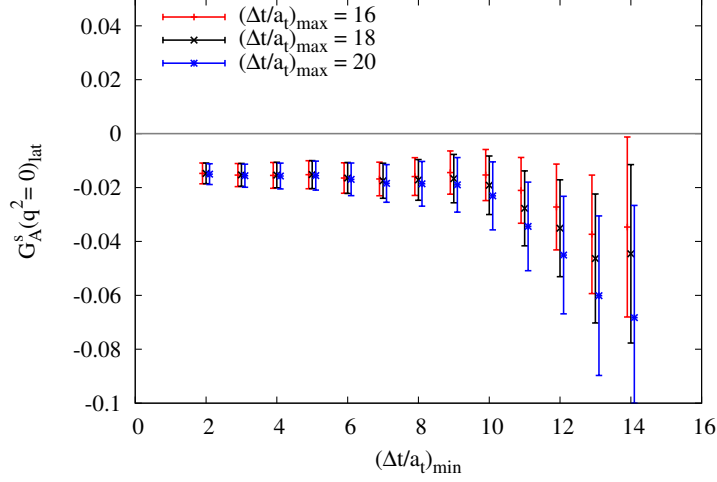


FIG. 12. Dependence of the extracted value of $G_A^s(Q^2=0)_{\text{lat}}$ on the range of time separations included in the fit.

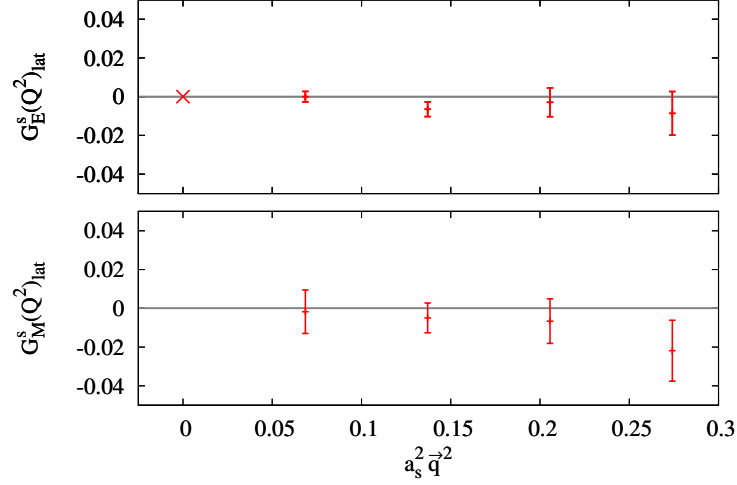


FIG. 13. Strange electric and magnetic form factors as a function of momentum.

given by

$$Q^2 = 2M_N \left(\sqrt{|\vec{q}|^2 + M_N^2} - M_N \right), \quad (33)$$

where M_N is our lattice determination of the nucleon mass. The quoted errors for Q^2 reflect the uncertainties in M_N and the lattice scale. We again emphasize that the results in Table I were determined with $m_{u,d}$ unphysically heavy, corresponding to a pion mass of about 400 MeV, and that the tabulated values for $G_S^s(Q^2)$ and $G_A^s(Q^2)$ are unrenormalized.

V. CONCLUSION

In this work, we have described our first effort to compute disconnected contributions to nucleon form factors, focusing on the strange quark. Employing the Wilson gauge and fermion actions on an anisotropic lattice, we computed a large number of nucleon correlators and accurate unbiased estimates for the disconnected currents on each gauge

$(L_s/2\pi)^2 \vec{q} ^2$	Q^2 [GeV ²]	$G_S^s(Q^2)_{\text{lat}}$	$G_A^s(Q^2)_{\text{lat}}^{(\text{p.s.})}$	$G_A^s(Q^2)_{\text{lat}}^{(\text{local})}$	$G_E^s(Q^2)_{\text{lat}}$	$G_M^s(Q^2)_{\text{lat}}$
0	0	2.84(49)	-0.019(11)	-0.024(15)	—	—
1	0.22(3)	1.59(34)	-0.002(7)	-0.008(10)	0.000(3)	-0.002(11)
2	0.43(5)	1.20(28)	-0.003(6)	-0.006(9)	-0.007(4)	-0.005(8)
3	0.62(8)	0.49(43)	-0.001(11)	-0.005(16)	-0.003(7)	-0.007(12)
4	0.81(10)	-0.31(62)	-0.012(15)	-0.012(22)	-0.009(11)	-0.022(16)

TABLE I. Summary of results for strange form factors of the nucleon.

configuration. We nevertheless found results for the electromagnetic form factors that are consistent with zero and a result for Δs that is only marginally distinct from zero, suggesting that the physical values of these quantities are rather small. Such null results may be interpreted as limits — with the aforementioned caveats concerning systematics — and should also be useful for setting bounds on the disconnected contributions that are generally neglected in lattice determinations of nucleon form factors (or explicitly canceled by taking isovector combinations). To complete this program, it will of course be necessary to include disconnected contributions from light quarks as well.

In the future, we plan to build on the present investigation by introducing several improvements. First, we are making use of multiple ensembles of anisotropic lattices with 2+1 flavors in the sea [60], which will allow the strange quark to be treated fully self-consistently. These were generated with a Wilson fermion action that is stout-smear [61] and $O(a)$ -improved [62], both features that may be expected to improve the chiral properties of the action [63] and thereby reduce the effect of flavor mixing discussed in Section IV A. Indeed, the fact that their action is clover-improved may explain why the authors of [35] found a value for $\langle N|\bar{s}s|N\rangle_0$ that is significantly smaller than ours (but still larger than determinations employing chiral or staggered fermions); one must also take multiplicative renormalization factors into account when comparing bare values obtained with different actions, but such factors are not expected to differ enough from unity to account for the discrepancy. These new ensembles also have a much longer extent in time (with volumes of $24^3 \times 128$ and larger), which will suppress contaminations from backward-propagating states and allow us to obtain a signal over a larger range of time separations, thus reducing statistical errors.

Second, we are leveraging a powerful new adaptive multigrid (MG) algorithm for inverting the Wilson-clover Dirac operator that is allowing us to compute the disconnected diagrams for both strange and light quarks at very little additional cost [64, 65]. We are also taking advantage of clusters accelerated by graphics processing units (GPUs) using the QUDA library [66, 67], which provides another substantial speedup. Work is underway to develop an MG implementation suitable for GPUs, in lieu of the Krylov solvers currently implemented in QUDA. We estimate that by combining these two improvements, we may be able to reduce the cost per Dirac inversion at light quark masses by up to two orders of magnitude as compared to standard solvers on traditional architectures. Finally, we are exploring additional methods for reducing the variance in estimates of the trace of disconnected currents, such as the multigrid subtraction method described in [45]. The net result of these improvements will be a significant reduction in both statistical and systematic errors. At the same time, the scheme outlined in Appendix C should allow us to correct for operator mixing in the determination of the strange scalar matrix element, yielding a reliable value and further elucidating the connection between results obtained with chiral and Wilson-like fermions.

ACKNOWLEDGMENTS

We wish to acknowledge useful discussions with Joel Giedt and Stephen Sharpe. This work was supported in part by U.S. DOE grants DE-FG02-91ER40676 and DE-FC02-06ER41440; NSF grants DGE-0221680, PHY-0427646, and PHY-0835713; and by the NSF through TeraGrid resources provided by the Texas Advanced Computing Center [68]. Computations were also carried out on facilities of the USQCD Collaboration, which are funded by the Office of Science of the U.S. Department of Energy, as well as on the Scientific Computing Facilities of Boston University.

Appendix A: The Wilson action for an anisotropic lattice

In our calculation, we take the temporal lattice spacing a_t to be finer than that in the three spatial directions, which share a common value a_s . In the interacting theory, the anisotropy $\xi \equiv a_s/a_t$ renormalizes away from the bare value that appears in the action, which we denote by ξ_0 . Furthermore, the anisotropies appearing in the gauge and fermion actions may in principle renormalize differently. We follow [50] in denoting the bare gauge anisotropy by ξ_0

while introducing a new parameter ν such that the bare fermion anisotropy is given by ξ_0/ν . We assume that the renormalization of the latter quantity is independent of quark mass, as found empirically in [50, 69].

With these definitions, the Wilson gauge action on an anisotropic lattice is given by [70]

$$S_g = \frac{6}{\xi_0 g^2} \sum_x \sum_{\mu=1}^3 \left[\sum_{\nu < \mu < 4} \left(1 - \frac{1}{3} \text{Re } U_{\mu\nu}(x) \right) + \xi_0^2 \left(1 - \frac{1}{3} \text{Re } U_{\mu 4}(x) \right) \right], \quad (\text{A1})$$

in terms of the plaquette $U_{\mu\nu}(x) = \text{Tr} [U_\mu(x) U_\nu(x + a_\mu \hat{\mu}) U_\mu^\dagger(x + a_\nu \hat{\nu}) U_\nu^\dagger(x)]$, where $\mu = 4$ corresponds to the “time” direction. The Wilson fermion action, in turn, is given by [71]

$$S_W = a_s^3 \sum_x \bar{\psi}(x) \left[a_t m_q^0 + \frac{\nu}{\xi_0} a_s \sum_{i=1}^3 \left(\frac{1}{2} \gamma_i (\nabla_i + \nabla_i^*) - \frac{a_s}{2} \nabla_i^* \nabla_i \right) + a_t \left(\frac{1}{2} \gamma_4 (\nabla_4 + \nabla_4^*) - \frac{a_t}{2} \nabla_4^* \nabla_4 \right) \right] \psi(x), \quad (\text{A2})$$

where we have defined the covariant difference operators $\nabla_\mu \psi(x) = [U_\mu(x) \psi(x + a_\mu \hat{\mu}) - \psi(x)]/a_\mu$ and $\nabla_\mu^* \psi(x) = [\psi(x) - U_\mu^\dagger(x - a_\mu \hat{\mu}) \psi(x - a_\mu \hat{\mu})]/a_\mu$. Note that a_t occurs in Eq. (A2) only to cancel where it appears in the definition of ∇_4 , except in the dimensionless mass parameter ($a_t m_q^0$). We can write the fermion action in a more familiar and explicit form by defining rescaled links,

$$\tilde{U}_\mu(x) = \begin{cases} \frac{\nu}{\xi_0} U_\mu(x) & \text{for } \mu = 1, 2, 3 \\ U_\mu(x) & \text{for } \mu = 4, \end{cases} \quad (\text{A3})$$

and defining

$$\frac{1}{2\kappa} = \left(a_t m_q^0 + \frac{3\nu}{\xi_0} + 1 \right). \quad (\text{A4})$$

Thus we have $S_W = a_s^3 \sum_x \bar{\psi} D \psi(x)$, where

$$D \psi(x) = \frac{1}{2\kappa} \psi(x) - \frac{1}{2} \sum_{\mu=1}^4 \left[(1 - \gamma_\mu) \tilde{U}_\mu(x) \psi(x + \hat{\mu}) + (1 + \gamma_\mu) \tilde{U}_\mu^\dagger(x - \hat{\mu}) \psi(x - \hat{\mu}) \right]. \quad (\text{A5})$$

(For convenience, we have also redefined $a_\mu \hat{\mu} \rightarrow \hat{\mu}$.) Note that we have kept the continuum normalization of the fermion field $\psi(x)$.

Appendix B: Quark mass determination

Due to the explicit breaking of chiral symmetry in the Wilson action, the naive quark mass m_q^0 that appears in Eq. (A2) is not protected from additive shifts under renormalization. In Section IV A, we require the subtracted bare mass, $\tilde{m}_s^0 = m_s^0 - m_{\text{crit}}$, where the critical mass m_{crit} corresponds to the value of m_0 at which the physical quark mass vanishes. The naive mass for the strange quark is a parameter of the theory; it has been chosen such that the mass of the ϕ meson calculated on the lattice reproduces the physical value [50]. To determine m_{crit} , we utilize the dependence of the (partially quenched) pseudoscalar meson mass M_P on the valence quark mass: $M_P^2 = 2Bm_l^{\text{val}}$ to leading order in partially quenched chiral perturbation theory. The critical mass so defined depends implicitly on the fixed sea quark mass [72, 73]. As advocated in [74], a reasonable approach is to determine m_{crit} for each available value of the light sea quark mass m_l^{sea} and then extrapolate to the physical point where $m_l^{\text{sea}} = m_{u,d}$. (Alternatively, one could fit all available data for M_P^2 to a functional form that incorporates the dependence on both the sea and valence quark masses [55].) Consistent with the other results presented in this work, because only a single value of m_l^{sea} is available, we do not perform this final extrapolation in the light sea quark mass.

Figure 14 illustrates our determination of the critical mass. For each of seven valence quark masses, we evaluated pseudoscalar correlators on an ensemble of 216 gauge configurations. The corresponding meson masses were determined from a single-cosh fit in the range $20 \leq t/a_t \leq 44$. Upon performing a linear extrapolation in the quark mass, we find $a_t m_{\text{crit}} = -0.42116(24)$, where the statistical error has been estimated via jackknife. Given the naive mass that was input for the strange quark, $a_t m_s^0 = -0.38922$, we find $a_t \tilde{m}_s^0 = 0.03194(24)$ for the subtracted bare strange quark mass.

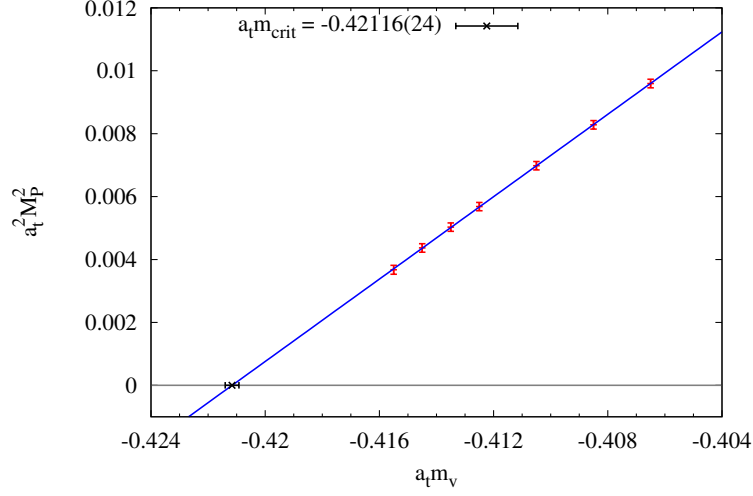


FIG. 14. Mass of the pseudoscalar meson squared, as a function of the valence quark mass.

Appendix C: Flavor mixing for Wilson quarks

In principle to extract continuum quantities, one must take the lattice spacing (i.e., the bare coupling) to zero holding renormalized parameters fixed, even for renormalization group invariant quantities such as ratios of masses. However, better estimates can often be found at finite lattice spacing by “renormalizing” the bare lattice quantities. A particularly interesting and difficult quantity for Wilson fermions is the continuum parameter for the Higgs coupling to the strange quark content of the nucleon,

$$f_{Ts} = \frac{m_s \langle N | \bar{s}s | N \rangle}{M_N} = m_s \frac{\partial}{\partial m_s} \log[M_N]. \quad (C1)$$

The expression on the right is an identity based on the Feynman-Hellmann theorem with the partial derivative taken with respect to the renormalized strange quark mass, holding the renormalized light quark mass and scale fixed. For Wilson quarks on the lattice, mixing with the light quark condensates in the nucleon can produce a large contribution to f_{Ts} , as pointed out by Michael, McNeile, and Hepburn [38]. To understand this, let us consider a mass-independent renormalization scheme on the lattice. We note that very similar methods are employed in Section IV.B of [56], despite some differences in the choice of the lattice renormalization scheme. For convenience, in this Appendix, we adopt a convention where lattice mass parameters are dimensionless. Also we will consider only the more physically relevant case of 2 + 1 flavors, even though our present results are calculated on 2 flavor gauge configurations. There is however still non-zero mixing in the 2 flavor case as illustrated in Figure 7 to lowest order.

For Wilson quarks there are two important issues not present for a chiral formulation. First, we have additive mass renormalization, which requires that a constant be subtracted from the bare quark mass. Second, the disconnected diagram for the mass insertion operator $\bar{\psi}\psi = \bar{\psi}_L\psi_R + \bar{\psi}_R\psi_L$ does not vanish even when the subtracted quark masses vanish. We begin by rewriting the mass term in the lattice Lagrangian in terms of singlet, $m_S^0 = (2m_l^0 + m_s^0)/3$, and non-singlet, $m_{NS}^0 = (m_l^0 - m_s^0)/\sqrt{3}$, masses:

$$\mathcal{L}_m = m_l^0(\bar{u}u + \bar{d}d) + m_s^0\bar{s}s = m_S^0\bar{\psi}\psi + m_{NS}^0\bar{\psi}\lambda_8\psi, \quad (C2)$$

where for simplicity we take degenerate light quarks $m_l^0 = m_u^0 = m_d^0$. The singlet and non-singlet masses renormalize differently because of the lack of chiral symmetry. The renormalization scheme we choose is

$$\begin{aligned} m_S &= Z_0^m(g_0)(m_S^0 - m_{\text{crit}}(g_0))/a, \\ m_{NS} &= Z_8^m(g_0)m_{NS}^0/a, \\ \Lambda &= \Lambda^0(g_0)/a. \end{aligned} \quad (C3)$$

The first two equations define the renormalized masses, while the last defines some renormalized scale which, for simplicity, we will take to depend on the lattice spacing and some function of only the bare coupling. There are many

possible choices for Λ , such as the rho mass or pion decay constant, though it will not enter into our final results so we leave it unspecified. We have also introduced the lattice spacing, a , to convert quantities to physical units. This needs to be set by comparing some lattice measurement with a physical value. One choice would be to set the lattice spacing using the Sommer scale, r_0 [51], as

$$a = r_0^{phys} / r_0^{lat}(g_0) \quad (C4)$$

where r_0^{lat} is the dimensionless value measured on each lattice ensemble and r_0^{phys} is some reference value in physical units. As with Λ , the exact choice of definition for a is irrelevant for the present discussion. Here we have made these quantities independent of the masses. One could systematically improve on this by adding extra terms with increasing powers of the subtracted masses, but, for simplicity, we will not include these.

The mass renormalizations above can be expressed in terms of the light and strange quarks themselves,

$$\begin{aligned} m_l &= m_S + m_{NS}/\sqrt{3} = \frac{1}{3} [(2Z_0^m + Z_8^m)\tilde{m}_l^0 + (Z_0^m - Z_8^m)\tilde{m}_s^0] / a, \\ m_s &= m_S - 2m_{NS}/\sqrt{3} = \frac{1}{3} [(Z_0^m + 2Z_8^m)\tilde{m}_s^0 + 2(Z_0^m - Z_8^m)\tilde{m}_l^0] / a, \end{aligned} \quad (C5)$$

where $\tilde{m}_i^0 = m_i^0 - m_{crit}$. We are now ready to find the expression for renormalized condensates. Due to the vector Ward identity the non-singlet operator renormalizes as

$$(\bar{\psi}\lambda_8\psi)^R = Z_8(\bar{\psi}\lambda_8\psi)^{lat}, \quad (C6)$$

where $Z_8 = 1/Z_8^m$, but the singlet piece is unconstrained by vector current conservation. However we can uniquely determine the renormalization of the condensates by evaluating the Feynman-Hellmann theorem,

$$f_{Ts} = m_s \frac{\partial}{\partial m_s} \log[a^{-1}M_N^0], \quad (C7)$$

(where $M_N^0 = aM_N$ is the nucleon mass in lattice units) in terms of bare lattice parameters. The partial derivative is expanded as

$$\left. \frac{\partial}{\partial m_s} \right|_{m_l, \Lambda} = \frac{\partial m_s^0}{\partial m_s} \frac{\partial}{\partial m_s^0} + \frac{\partial m_l^0}{\partial m_s} \frac{\partial}{\partial m_l^0} + \frac{\partial g_0^{-2}}{\partial m_s} \frac{\partial}{\partial g_0^{-2}}, \quad (C8)$$

leading to the expression

$$f_{Ts} = m_s \left[\frac{\partial m_s^0}{\partial m_s} \langle N | \bar{s}s | N \rangle_0 + \frac{\partial m_l^0}{\partial m_s} \langle N | \bar{u}u + \bar{d}d | N \rangle_0 + \frac{\partial g_0^{-2}}{\partial m_s} \left(\langle N | g_0^2 S_g | N \rangle_0 + a \frac{\partial a^{-1}}{\partial g_0^{-2}} M_N^0 \right) \right] / M_N^0 \quad (C9)$$

where S_g is the gauge action and $\langle . \rangle_0$ is an unrenormalized lattice matrix element.

Finally, using the renormalization scheme in (C3), we evaluate the coefficients in this expression by use of the implicit function theorem, inverting the Jacobian matrix

$$\frac{\partial(m_l, m_s, \Lambda)}{\partial(m_l^0, m_s^0, g_0^{-2})} = \begin{bmatrix} \frac{\partial m_l}{\partial m_l^0} & \frac{\partial m_l}{\partial m_s^0} & \frac{\partial m_l}{\partial g_0^{-2}} \\ \frac{\partial m_s}{\partial m_l^0} & \frac{\partial m_s}{\partial m_s^0} & \frac{\partial m_s}{\partial g_0^{-2}} \\ 0 & 0 & \frac{\partial \Lambda}{\partial g_0^{-2}} \end{bmatrix}. \quad (C10)$$

From Eq. (C5) the determinant is then given by

$$J = \frac{\partial \Lambda}{\partial g_0^{-2}} \left[\frac{\partial m_l}{\partial m_l^0} \frac{\partial m_s}{\partial m_s^0} - \frac{\partial m_l}{\partial m_s^0} \frac{\partial m_s}{\partial m_l^0} \right] = \frac{\partial \Lambda}{\partial g_0^{-2}} Z_0^m Z_8^m / a^2. \quad (C11)$$

Matrix elements of the inverse of the Jacobian are thus given by

$$\begin{aligned} \frac{\partial m_s^0}{\partial m_s} &= J^{-1} \frac{\partial \Lambda}{\partial g_0^{-2}} \frac{\partial m_l}{\partial m_l^0} = \frac{a}{3} \left[\frac{1}{Z_0^m} + \frac{2}{Z_8^m} \right], \\ \frac{\partial m_l^0}{\partial m_s} &= -J^{-1} \frac{\partial \Lambda}{\partial g_0^{-2}} \frac{\partial m_l}{\partial m_s^0} = \frac{a}{3} \left[\frac{1}{Z_0^m} - \frac{1}{Z_8^m} \right], \\ \frac{\partial g_0^{-2}}{\partial m_s} &= 0. \end{aligned} \quad (C12)$$

Thus we identify $Z_0 = 1/Z_0^m$ and $Z_8 = 1/Z_8^m$ to obtain a form similar to Eq. (29) in the main text,

$$f_{Ts} = \frac{m_s}{3M_N} \left[(Z_0 + 2Z_8) \langle N | \bar{s}s | N \rangle_0 + (Z_0 - Z_8) \langle N | \bar{u}u + \bar{d}d | N \rangle_0 \right]. \quad (\text{C13})$$

It is interesting that here the relations $Z_i = 1/Z_i^m$ did not involve the use of Ward identities, contrary to standard derivations. Also note that there is no $\langle N | g_0^2 S_g | N \rangle_0$ contribution to this order in the renormalization scheme. However as emphasized in [56], it may be important to include additional $O(am_s)$ corrections which will cause $\partial g_0^{-2}/\partial m_s$ to no longer vanish and will induce operator mixing with $\langle N | S_g | N \rangle_0$. Since on dimensional and RG grounds this term is $O(am_s g_0^2)$, it should be relatively small. The mixing with the light valence quarks is substantial and with the estimate for $Z_8/Z_0 > 1$, it will tend to cancel the contribution from $\langle N | \bar{s}s | N \rangle_0$ found for the bare amplitude. To see this in more detail, note that renormalizing f_{Ts} also requires finding the renormalized strange quark mass,

$$m_s = \frac{1}{3} \left[(Z_0^m + 2Z_8^m) \tilde{m}_s^0 + 2(Z_0^m - Z_8^m) \tilde{m}_l^0 \right] / a. \quad (\text{C14})$$

Consequently, the dimensionless ratio f_{Ts} only depends on the ratio $Z_0^m/Z_8^m = Z_8/Z_0$, which can be computed by a procedure described in detail in [54, 55] in the context of quark masses. It is convenient to rewrite the expression as

$$f_{Ts} = \frac{\tilde{m}_s^0 + 2\Delta(\tilde{m}_l^0 - \tilde{m}_s^0)/[3(1 + \Delta)]}{M_N^0} \left[\langle N | \bar{s}s | N \rangle_0 - \Delta \langle N | (\bar{u}u + \bar{d}d - 2\bar{s}s) | N \rangle_0 / 3 \right], \quad (\text{C15})$$

in terms of an operator mixing parameter $\Delta = Z_8/Z_0 - 1$. The mixing term is a pure non-singlet operator, $\Delta \bar{\psi} \lambda_8 \psi / \sqrt{3}$. The disconnected contribution to $\bar{\psi} \lambda_8 \psi / \sqrt{3}$ vanishes like $O(am_i)$ in the chiral limit, but the valence contribution remains large at current lattice spacings, resulting in a correction of the same order of magnitude as the bare matrix element given in the text: $a^{-1} \tilde{m}_s^0 \langle N | \bar{s}s | N \rangle_0 \simeq 504(91)(30)$ MeV.

-
- [1] D. H. Beck and R. D. McKeown, Ann. Rev. Nucl. Part. Sci. **51**, 189 (2001), arXiv:hep-ph/0102334
 - [2] M. J. Ramsey-Musolf, Eur. Phys. J. **A24S2**, 197 (2005), arXiv:nucl-th/0501023
 - [3] J. Liu, R. D. McKeown, and M. J. Ramsey-Musolf, Phys. Rev. **C76**, 025202 (2007), arXiv:0706.0226 [nucl-ex]
 - [4] R. D. Young, J. Roche, R. D. Carlini, and A. W. Thomas, Phys. Rev. Lett. **97**, 102002 (2006), arXiv:nucl-ex/0604010
 - [5] L. A. Ahrens *et al.*, Phys. Rev. **D35**, 785 (1987)
 - [6] S. F. Pate, D. W. McKee, and V. Papavassiliou, Phys. Rev. **C78**, 015207 (2008), arXiv:0805.2889 [hep-ex]
 - [7] A. A. Aguilar-Arevalo *et al.* (MiniBooNE) (2010), arXiv:1007.4730 [hep-ex]
 - [8] S. E. Kuhn, J. P. Chen, and E. Leader, Prog. Part. Nucl. Phys. **63**, 1 (2009), arXiv:0812.3535 [hep-ph]
 - [9] A. Airapetian *et al.* (HERMES), Phys. Rev. **D75**, 012007 (2007), arXiv:hep-ex/0609039
 - [10] A. Airapetian *et al.* (HERMES), Phys. Lett. **B666**, 446 (2008), arXiv:0803.2993 [hep-ex]
 - [11] J. Gasser, H. Leutwyler, and M. E. Sainio, Phys. Lett. **B253**, 252 (1991)
 - [12] A. Bottino, F. Donato, N. Fornengo, and S. Scopel, Astropart. Phys. **18**, 205 (2002), arXiv:hep-ph/0111229
 - [13] J. R. Ellis, K. A. Olive, Y. Santoso, and V. C. Spanos, Phys. Rev. **D71**, 095007 (2005), arXiv:hep-ph/0502001
 - [14] E. A. Baltz, M. Battaglia, M. E. Peskin, and T. Wizansky, Phys. Rev. **D74**, 103521 (2006), arXiv:hep-ph/0602187
 - [15] J. R. Ellis, K. A. Olive, and C. Savage, Phys. Rev. **D77**, 065026 (2008), arXiv:0801.3656 [hep-ph]
 - [16] A. E. Nelson and D. B. Kaplan, Phys. Lett. **B192**, 193 (1987)
 - [17] D. B. Kaplan and A. Manohar, Nucl. Phys. **B310**, 527 (1988)
 - [18] J. Giedt, A. W. Thomas, and R. D. Young, Phys. Rev. Lett. **103**, 201802 (2009), arXiv:0907.4177 [hep-ph]
 - [19] J. M. Zanotti, PoS **LATTICE2008**, 007 (2008), arXiv:0812.3845 [hep-lat]
 - [20] C. Alexandrou, PoS **LATTICE2010**, 001 (2010), arXiv:1011.3660 [hep-lat]
 - [21] M. Fukugita, Y. Kuramashi, M. Okawa, and A. Ukawa, Phys. Rev. Lett. **75**, 2092 (1995), arXiv:hep-lat/9501010
 - [22] M. Fukugita, Y. Kuramashi, M. Okawa, and A. Ukawa, Phys. Rev. **D51**, 5319 (1995), arXiv:hep-lat/9408002
 - [23] S. J. Dong, J. F. Lagaë, and K. F. Liu, Phys. Rev. Lett. **75**, 2096 (1995), arXiv:hep-ph/9502334
 - [24] S. J. Dong, J. F. Lagaë, and K. F. Liu, Phys. Rev. **D54**, 5496 (1996), arXiv:hep-ph/9602259
 - [25] S. J. Dong, K. F. Liu, and A. G. Williams, Phys. Rev. **D58**, 074504 (1998), arXiv:hep-ph/9712483
 - [26] S. Güsken *et al.* (TXL), Phys. Rev. **D59**, 054504 (1999), arXiv:hep-lat/9809066
 - [27] S. Güsken *et al.* (TXL), Phys. Rev. **D59**, 114502 (1999)
 - [28] N. Mathur and S.-J. Dong (Kentucky Field Theory), Nucl. Phys. Proc. Suppl. **94**, 311 (2001), arXiv:hep-lat/0011015
 - [29] R. Lewis, W. Wilcox, and R. M. Woloshyn, Phys. Rev. **D67**, 013003 (2003), arXiv:hep-ph/0210064
 - [30] T. Doi *et al.*, Phys. Rev. **D80**, 094503 (2009), arXiv:0903.3232 [hep-ph]
 - [31] R. Babich *et al.*, PoS **LATTICE2008**, 160 (2008), arXiv:0901.4569 [hep-lat]
 - [32] G. Bali, S. Collins, and A. Schafer, PoS **LATTICE2008**, 161 (2008), arXiv:0811.0807 [hep-lat]

- [33] G. S. Bali, S. Collins, and A. Schafer, *Comput. Phys. Commun.* **181**, 1570 (2010), arXiv:0910.3970 [hep-lat]
- [34] G. Bali, S. Collins, and A. Schafer (QCDSF), *PoS LAT2009*, 149 (2009), arXiv:0911.2407 [hep-lat]
- [35] S. Collins *et al.*, *PoS LATTICE2010*, 134 (2010), arXiv:1011.2194 [hep-lat]
- [36] D. Toussaint and W. Freeman (MILC), *Phys. Rev. Lett.* **103**, 122002 (2009), arXiv:0905.2432 [hep-lat]
- [37] K. Takeda *et al.* (JLQCD)(2010), arXiv:1011.1964 [hep-lat]
- [38] C. Michael, C. McNeile, and D. Hepburn (UKQCD), *Nucl. Phys. Proc. Suppl.* **106**, 293 (2002), arXiv:hep-lat/0109028
- [39] H. Ohki *et al.*, *Phys. Rev.* **D78**, 054502 (2008), arXiv:0806.4744 [hep-lat]
- [40] H. Ohki *et al.*, *PoS LAT2009*, 124 (2009), arXiv:0910.3271 [hep-lat]
- [41] R. D. Young and A. W. Thomas, *Phys. Rev.* **D81**, 014503 (2010), arXiv:0901.3310 [hep-lat]
- [42] D. B. Leinweber *et al.*, *Phys. Rev. Lett.* **94**, 212001 (2005), arXiv:hep-lat/0406002
- [43] D. B. Leinweber *et al.*, *Phys. Rev. Lett.* **97**, 022001 (2006), arXiv:hep-lat/0601025
- [44] P. Wang, D. B. Leinweber, A. W. Thomas, and R. D. Young, *Phys. Rev.* **C79**, 065202 (2009), arXiv:0807.0944 [hep-ph]
- [45] R. Babich *et al.*, *PoS LAT2007*, 139 (2007), arXiv:0710.5536 [hep-lat]
- [46] S.-J. Dong and K.-F. Liu, *Phys. Lett.* **B328**, 130 (1994), arXiv:hep-lat/9308015
- [47] J. Viehoff *et al.* (TXL), *Nucl. Phys. Proc. Suppl.* **63**, 269 (1998), arXiv:hep-lat/9710050
- [48] S. Bernardson, P. McCarty, and C. Thron, *Comput. Phys. Commun.* **78**, 256 (1993)
- [49] J. Foley *et al.*, *Comput. Phys. Commun.* **172**, 145 (2005), arXiv:hep-lat/0505023
- [50] J. M. Bulava *et al.*, *Phys. Rev.* **D79**, 034505 (2009), arXiv:0901.0027 [hep-lat]
- [51] R. Sommer, *Nucl. Phys.* **B411**, 839 (1994), arXiv:hep-lat/9310022
- [52] C. Aubin *et al.*, *Phys. Rev.* **D70**, 094505 (2004), arXiv:hep-lat/0402030
- [53] C. Bernard *et al.* (MILC), *PoS LAT2006*, 163 (2006), arXiv:hep-lat/0609053
- [54] P. E. L. Rakow, *Nucl. Phys. Proc. Suppl.* **140**, 34 (2005), arXiv:hep-lat/0411036
- [55] M. Gockeler *et al.* (QCDSF), *Phys. Lett.* **B639**, 307 (2006), arXiv:hep-ph/0409312
- [56] T. Bhattacharya, R. Gupta, W. Lee, S. R. Sharpe, and J. M. S. Wu, *Phys. Rev.* **D73**, 034504 (2006), arXiv:hep-lat/0511014
- [57] K. Jansen *et al.*, *Phys. Lett.* **B372**, 275 (1996), arXiv:hep-lat/9512009
- [58] M. Lüscher and P. Weisz, *Nucl. Phys.* **B479**, 429 (1996), arXiv:hep-lat/9606016
- [59] S. Baunack *et al.*, *Phys. Rev. Lett.* **102**, 151803 (2009), arXiv:0903.2733 [nucl-ex]
- [60] H.-W. Lin *et al.* (Hadron Spectrum), *Phys. Rev.* **D79**, 034502 (2009), arXiv:0810.3588 [hep-lat]
- [61] C. Morningstar and M. J. Peardon, *Phys. Rev.* **D69**, 054501 (2004), arXiv:hep-lat/0311018
- [62] B. Sheikholeslami and R. Wohlert, *Nucl. Phys.* **B259**, 572 (1985)
- [63] S. Capitani, S. Durr, and C. Hoelbling, *JHEP* **11**, 028 (2006), arXiv:hep-lat/0607006
- [64] R. Babich *et al.*, *Phys. Rev. Lett.* **105**, 201602 (2010), arXiv:1005.3043 [hep-lat]
- [65] J. C. Osborn *et al.*, *PoS LATTICE2010*, 037 (2010), arXiv:1011.2775 [hep-lat]
- [66] M. A. Clark, R. Babich, K. Barros, R. C. Brower, and C. Rebbi, *Comput. Phys. Commun.* **181**, 1517 (2010), arXiv:0911.3191 [hep-lat]
- [67] R. Babich, M. A. Clark, and B. Joó, SC '10: Proceedings of the 2010 ACM/IEEE International Conference for High Performance Computing, Networking, Storage and Analysis(2010), doi:"bibinfo doi 10.1109/SC.2010.40, arXiv:1011.0024 [hep-lat]
- [68] C. Catlett *et al.*, *HPC and Grids in Action*, Amsterdam(2007)
- [69] R. G. Edwards, B. Joó, and H.-W. Lin, *Phys. Rev.* **D78**, 054501 (2008), arXiv:0803.3960 [hep-lat]
- [70] T. R. Klassen, *Nucl. Phys.* **B533**, 557 (1998), arXiv:hep-lat/9803010
- [71] T. R. Klassen, *Nucl. Phys. Proc. Suppl.* **73**, 918 (1999), arXiv:hep-lat/9809174
- [72] N. Eicker *et al.* (TXL), *Phys. Lett.* **B407**, 290 (1997), arXiv:hep-lat/9704019
- [73] S. R. Sharpe, *Phys. Rev.* **D56**, 7052 (1997), arXiv:hep-lat/9707018
- [74] T. Bhattacharya and R. Gupta, *Nucl. Phys. Proc. Suppl.* **63**, 95 (1998), arXiv:hep-lat/9710095